# CFD Analysis of C-D Nozzle Compared with Theoretical & Experimental Data

(Andrew) Stewart KEIR*,[1], Rob IVES[1], Faik HAMAD[1]

*Corresponding author
[1]School of Science & Engineering, Teesside University,
Middlesbrough, TS1 3BA, UK,
N3085595@live.tees.ac.uk*, M2084041@live.tees.ac.uk, F.Hamad@lives.tees.ac.uk

*Abstract: In modern Computational Fluid Dynamic (CFD) Analysis of Convergent-Divergent (C-D) Nozzles, current research has shown that, it is common practice to use either experimental or analytical results to predict the accuracy of the CFD models by comparison of the results. It is also commonly agreed, amongst the literature reviewed, that the CFD modelling software packages available do not accurately model turbulence for applications such as transonic C-D nozzles. This study aims to develop a theoretical approach for calculation of flow properties along the axis of the C-D nozzle based on the fundamental gas dynamic equations. The theoretical analyses is validated by experimental data. Then, the CFD model is used to simulate the experimental cases which are compared with the data from both theoretical analysis and experimental measurements. Then, the validated CFD model can be used for more complex analyses, representing more elaborate flow phenomena such as internal shockwaves and boundary layers. The geometry used in the analytical study and CFD simulations constructed to model the experimental rig. The [1, 2] analytical study is undertaken using isentropic and adiabatic relationships and the output of the analytical study, the 'shockwave location tool', is created. The results from the analytical study are then used to optimise the redesign an experimental rig to for more favorable placement of pressure taps and gain a much better representation of the shockwaves occurring in the divergent section of the nozzle. The results from the CFD model can then be directly compared other results in order to gauge the accuracy of each method of analysis. The validated model can then be used in order to create several, novel nozzle designs which may offer better performance and ease of manufacture and may present feasible improvements to existing high-speed flow applications.*

*Key Words: Convergent-DivergentNozzle, CFD Simulation, Shockwave-Boundary Layer Interaction, Experimental Study*

## 1. INTRODUCTION

The one-dimensional inviscid isentropic flow in a convergent-divergent nozzle is a classical problem, which has different flow regimes depending upon nozzle pressure ratio. The inviscid theory predicts a simple shock structure consisting of a normal shock followed by a smooth recovery to exit pressure in the divergence part of a choked nozzle for nozzle pressure ratio corresponding to the over-expanded flow regime. However, in real conditions, multi-dimensional flow and viscous effects like wall boundary layer and flow separation

drastically alter the flow in nozzle as discussed by a number of researchers [1], [2], [3]. The convergent–divergent nozzle attracts a large number of researchers since it was developed by the Swedish inventor Gustaf de Lavalin 1888 for use on a steam turbine. The research in this area increased significantly with developments in aerospace applications where the nozzle is used to accelerate hot exhaust to generate high thrust such as in Ramjets, scramjets, and rockets [4]. The modern advances in computing technology have allowed for a vast amount of new capabilities in computer modelling. This has been embraced by several sectors of engineering through the development of Computational Fluid Dynamics. CFD vastly reduces the time and cost spent on physical testing in conceptual design as results from validated models which can be used to take successful candidates through to consecutive design minimizing the traditional method of physical production/ testing. The main challenge with modern CFD is the capability of models representing extremely complex flow features.

### 1.1 Governing Equations

The following principle equations [5], [6], [7], [8], [9] are used in some form or another to study the flow characteristics as it is allowing the user to make assumptions and compute the different flow variables such as pressure, velocity, temperature and turbulence.

Continuity Equation

$$\frac{\partial \rho}{\partial t} + \frac{\partial}{\partial x_i}(\rho v) = 0 \tag{1}$$

Momentum Equation

$$\frac{D(\rho u_i)}{Dt} = -\frac{\partial P}{\partial x_i} + \frac{\partial}{\partial x_j}\left[\mu_{eff}\left(\frac{\partial u_i}{\partial x_j} + \frac{\partial u_j}{\partial x_i} - \frac{2\delta_{ij}\partial u_k}{3\partial x_k}\right)\right] + \frac{\partial\left(-\rho u_i' u_j'\right)}{\partial x_j} \tag{2}$$

It is at this point, Pougatch et al [8] recommends assuming that the total enthalpy is considered constant to account for the conservation of energy. Therefore,

$$H_g = C_P T + \frac{V^2}{2} + K \quad \rightarrow \quad Constant \tag{3}$$

The characteristics of the quasi-one dimensional flow can also be calculated at any point in the supersonic region, related to Mach number of the flow.

$$\rho = \rho_0 \left[1 + \left(\frac{\gamma - 1}{2}\right) M^2\right]^{\gamma - 1} \tag{4}$$

$$P = P_0 \left[1 + \left(\frac{\gamma - 1}{2}\right) M^2\right]^{\frac{\gamma - 1}{\gamma}} \tag{5}$$

$$T = T_0 \left[1 + \left(\frac{\gamma - 1}{2}\right) M^2\right] \tag{6}$$

### 1.2 Shockwave Theory

Throughout the divergent portion of the nozzle as the flow exceeds Mach number 1 into the supersonic flow regime, unless it is perfectly expanded, shockwaves are likely to be present in the flow and will disrupt its isentropic nature. Shockwaves in supersonic flow occur due to a build-up of pressure behind the shockwave.

An equation which computes the required 'Shock Wave Pressure' is supplied (below) by [10]. If the pressure is lower than the ambient pressure, a shock will occur in the supersonic flow.

$$P_{shock} = P_{exit}\left(\frac{2\gamma}{\gamma + 1}M_{exit}^2 - \frac{\gamma - 1}{\gamma + 1}\right) \tag{7}$$

Although not isentropic, the characteristics of the flow post-shock are a function of the flow approaching it. The Mach number after the shock can be calculated using the following equation provided by [11].

$$M_{after} = \sqrt{\frac{(\gamma - 1)M_{before}^2 + 2}{2\gamma M_{before}^2 - (\gamma - 1)}} \tag{8}$$

### 1.3 Shockwave – Boundary Layer Interaction (SBLI)

Interaction between the boundary layer and shockwaves within a compressible flow domain is a relatively new and scantily-researched field. The interaction between shock-waves and boundary layers in the flow's supersonic regime presents a point of interest due to the potential impact on the characteristics of the nozzle flow (at off-design conditions) as is recognised by [12].

As can be seen in the images provided by [13], the resultant shockwave is far removed from the stereotypical, planar shockwave. Houghton et al. [14] go onto explain that a pressure rise of this magnitude (due to the relatively high local Mach number) leads to a separation of the laminar boundary layer well before the position of the normal (main) shock.
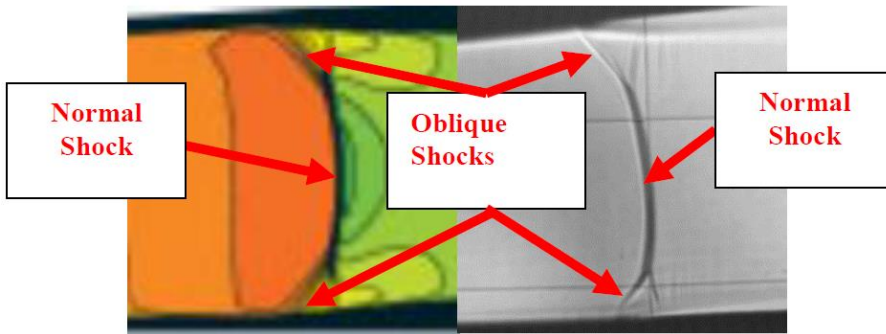


Figure 1 - Normal Shockwaves in Laval Nozzle after Interaction with Boundary Layers in both Simulation Form (Left) and Experimental 'Schlieren' Form (Right) [12]

The aim of this paper is twofold. The first is to study the behaviour of flow in C-D nozzle by analysing various parameters like static pressure, temperature, velocity and Mach number using analytical method based on fundamental gas dynamic equation, experimental measurements and CFD simulation. The second is to determine whether supersonic convergent-divergent nozzles can be accurately modelled through CFD simulation and validated via both theoretical and experimental data.

The initial work is to develop a theoretical approach for calculation of flow properties along the axis of the C-D nozzle based on the fundamental gas dynamic equations in the literature. The theoretical analyses are validated by comparison with experimental data. Then, the CFD model is used to model the experimental cases to predict the various variables which are compared with the data from both theoretical analysis and experimental

measurements from experimental rig developed in the jet engine lab. The validated CFD model is then used for more complex analyses, representing more elaborate flow phenomena such as internal shockwaves and boundary layers.

## 2. EXPERIMENTAL NOZZLE RIG

Figure 2 shows the schematic diagram of the nozzle rig used to collect the experimental data. The pressurised system air is introduced to the rig at the required inlet pressure through the red reservoir tank which is assumed to slow the flow to virtually stagnant (i.e. pressure and temperature in tank are assumed to be under stagnation conditions). The red tank acts as a stabilizer between the main compressors in the building and the nozzle inlet to minimize the fluctuation in air inlet conditions. The air then flows through the nozzle and past each pressure tapping where it is expanding through the diffuser.

The inlet pressure specified for the theoretical, experimental and CFD simulation are given in Table 1. The pressure transducers (C9553 COMARK) are connected to the test section by flexible plastic tubes to measure the pressure at a number of locations along the axis of the C-D nozzle.

### 2.1 Temperature Measurement

In order to record the temperature at each station, a thermocouple is inserted to pressure tappings at each station. This keeps the nozzle rig airtight and provides the necessary conditions to produce accurate temperature measurements. One type K thermocouple (0.5mm diameter) with an accuracy of ±0.25% is used to measure the temperature by a digital thermometer (RS 206-3738) with resolution of 0.1 $^{\circ}$C.

Table 1 - Inlet Pressures used in present investigation

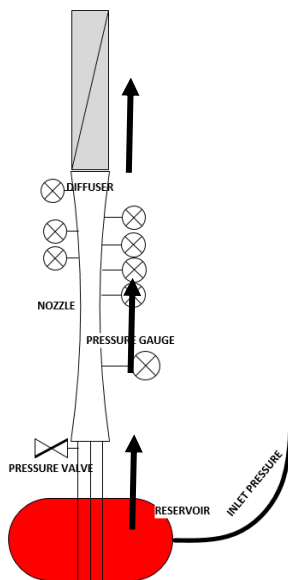| Test Number | Inlet Pressure |
|---|---|
| TEST 1 | 5.3 Bar (Gauge) |
| TEST 2 | 4.5 Bar (Gauge) |
| TEST 3 | 3.5 Bar (Gauge) |



Figure 2 - Schematic diagram of nozzle rig

## 3. SHOCKWAVE LOCATION TOOL

The geometry of the nozzle being analysed is based upon that of the experimental rig used throughout the research. The equations and methods used in this stream of work are given in [15]. The equations in this section are used to calculate the necessary isentropic properties of the nozzle at different axial positions. The shockwave location is determined, again by using several isentropic and shockwave-related equations in a novel fashion.

### 3.1 Shock Analysis Process

The likelihood of a shock being present can be summarised using Eq. (9). If the 'shock pressure' is lower than the ambient pressure, then it is highly likely that a shockwave will be present in the supersonic region of the flow, recovering enough pressure to adjust to ambient.

$$P_S = P_E \left( \frac{2\gamma}{\gamma + 1} M_E^2 - \frac{\gamma - 1}{\gamma + 1} \right) \tag{9}$$

***Step 1*** - Insert Initial Guess for Pressure before Shock (P$_{Before}$), Static pressure

Insert guess for static pressure at which the shock occurs, this process is iterative therefore this initial guess does not affect the results, but the amount of iterations required to get there.

***Step 2*** – Calculate Mach before Shock (*M$_{Before}$*)

Eq. (10) is used to calculate the Mach number of the flow immediately before the shock by assuming the isentropic flow condition. This will be based upon the initial guess for pressure.

$$M_{Before} = \sqrt{\frac{\left(\frac{P_{Before}}{P_T}\right)^{-\frac{\gamma-1}{\gamma}} \left(1 + \frac{\gamma-1}{2} M_{initial}^2\right) - 1}{\left(\frac{\gamma-1}{2}\right)}} \tag{10}$$

***Step 3*** – Calculate Area before Shock (*A$_{Before}$*)

Knowing *M$_{Before}$*, the *A$_{Before}$* can be calculated using the following equation Eq. (11) which is based upon a rearrangement of the Area-Ratio Mach Relationship.

$$A_{Before} = \frac{A_{initial} M_{initial}}{M_{before}} \left[ \frac{1 + \frac{\gamma-1}{2} M_{before}^2}{1 + \frac{\gamma-1}{2} M_{initial}^2} \right]^{\frac{\gamma+1}{2(\gamma-1)}} \tag{11}$$

***Step 4*** – Calculate the Mach number after Shock (*M$_{After}$*)

After the shockwave location in the nozzle, the static pressure spikes in order to adjust to the ambient pressure. As a result, the Mach number of the flow drops severely, the following equation Eq. (12) calculates the Mach number after the normal shockwave.

$$M_{after} = \sqrt{\frac{M_{before}^2 + \left(\frac{2}{\gamma-1}\right)}{\left(\frac{2\gamma}{\gamma-1}\right) M_{before}^2 - 1}} \tag{12}$$

***Step 5*** – Calculate the Static Pressure after Shock ($P_{After}$)

As mentioned in the previous step, the static pressure of the flow increases in order to adjust to ambient pressure at the latter stages of the nozzle. The static pressure after the shock is calculated using the following equation Eq. (13).

$$P_{after} = P_{before} \left[ \frac{1 + \gamma M_{before}^2}{1 + \gamma M_{after}^2} \right] \tag{13}$$

***Step 6*** – Calculate the Mach number at Nozzle Exit ($M_{exit}$)

Due to the assumption that normal shockwaves are extremely thin, the nozzle area before and after the shock can be considered identical.

By inserting $A_{exit}$, which is fixed, into the following equation Eq. (14) the Mach number at the nozzle exit can be computed.

$$M_{exit} = \frac{A_{before} M_{after}}{A_{exit}} \left[ \frac{1 + \frac{\gamma - 1}{2} M_{exit}^2}{1 + \frac{\gamma - 1}{2} M_{after}^2} \right]^{\frac{\gamma + 1}{2(\gamma - 1)}} \tag{14}$$

***Step 7*** – Calculate the Static Pressure at Nozzle Exit ($P_{exit}$)

The final step entails calculating the pressure at the nozzle exit through the usage of the following equation Eq. (15).

$$P_{exit} = P_{after} \left[ \frac{1 + \frac{\gamma - 1}{2} M_{after}^2}{1 + \frac{\gamma - 1}{2} M_{exit}^2} \right]^{\frac{\gamma}{\gamma - 1}} \tag{15}$$

The tool then uses an INDEX function in order to locate the optimum value (the smallest difference between calculated exit pressure and known ambient pressure). This function enables the user to find the area at which this 'optimum value' resides and, by cross-referencing this against the geometry data developed earlier, it can provide the axial position at which the shockwave is predicted to be.

## 4. CFD SIMULATION

The commercial code ANSYS Fluent (v17.4) was used to undertake the fluid simulation throughout this research. The fluid domain is modelled as thousands of smaller divisions (elements) where the variables for each are calculated individually. There are several considerations for the simulation process which affect the scope and quality of the model, they will be described and analysed throughout consecutive sections.

### 4.1 Mesh Selection

A successful mesh independence study provides a mesh that "arrives at the least number of elements that can yield accurate computational results" [16]. It is therefore advised, and undertaken, by various streams of research [5], [7], [8], [9], [17], [18],[19] to conduct a mesh independence study to ensure that the mesh being used provides the required flow features for the least penalty in computational time. Table 2 provides information regarding the meshes tested in the independence study.

Table 2 - Candidate meshes used throughout Mesh Convergence Study

| Mesh | Element Size (m) | Nodes | Elements |
|------|------------------|-------|----------|
| A | 0.001 | 281657 | 798326 |
| **B** | **0.0015** | **122531** | **302631** |
| C | 0.002 | 68511 | 156825 |
| D | 0.003 | 50763 | 110524 |

Based on the results produced using the different mesh sizes, Mesh "B" provides a sufficient level of accuracy, capturing the necessary flow features with a reasonable computation time. The Mach contours produced by different mesh are given in Figure 3 (which correspond to the values given in Table 2, above).
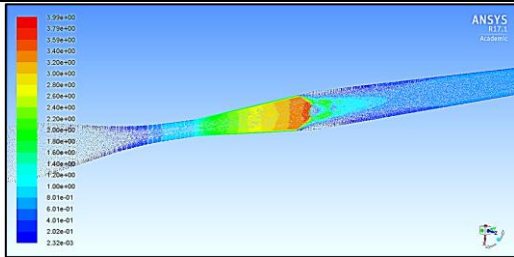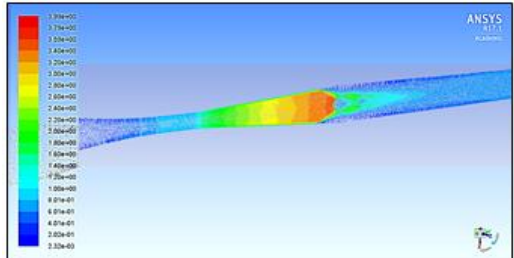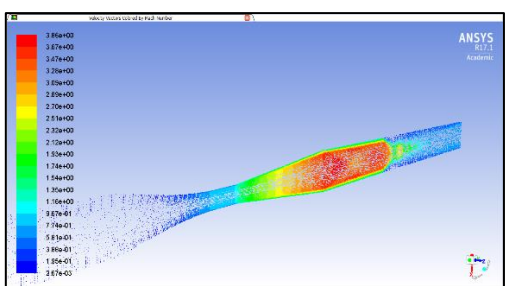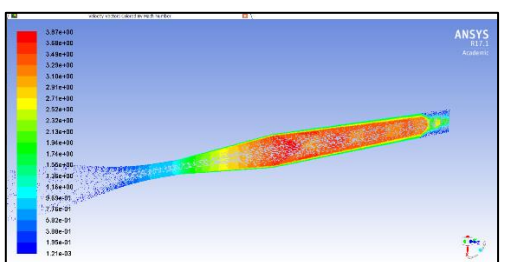
| Mesh | Elements | Mach Contour | Comments |
|------|----------|--------------|----------|
| **A** | **798,326** |  | • Menial increase in accuracy compared to Mesh B.<br>• Much larger computation time than Mesh B (around 2x longer). |
| **B** | **302,631** |  | • Provides a sufficient level of accuracy, capturing the necessary flow features with a reasonable computation time.<br>• Recommended for use. |
| **C** | **156,825** |  | • No clear production of shock region, flow appears to 'neck' downstream of expected shock region.<br>• Menial decrease in computational time compared to Mesh B. |
| **D** | **110,524** |  | • No real represntation of shock anywhere in fluid domain.<br>• Marked increase in set-up and computation time compared to other meshes but lack of accuracy mitigates this mesh being used. |

Figure 3 - Mach contours fordifferent number of elements

## 5. RESULTS & DISCUSSIONS

This section contains the combined the results, consisting of the Shockwave Tool, Fluent CFD and Experimental Results. The experimental results are represented by data points, as opposed to curves, due to their only being only 8 data collection points on the experimental nozzle rig. The temperature and pressure values are raw data collected from measuring devices however the Mach number values are calculated from temperature, pressure and velocity data measured along with some well-established laws of gas dynamics.
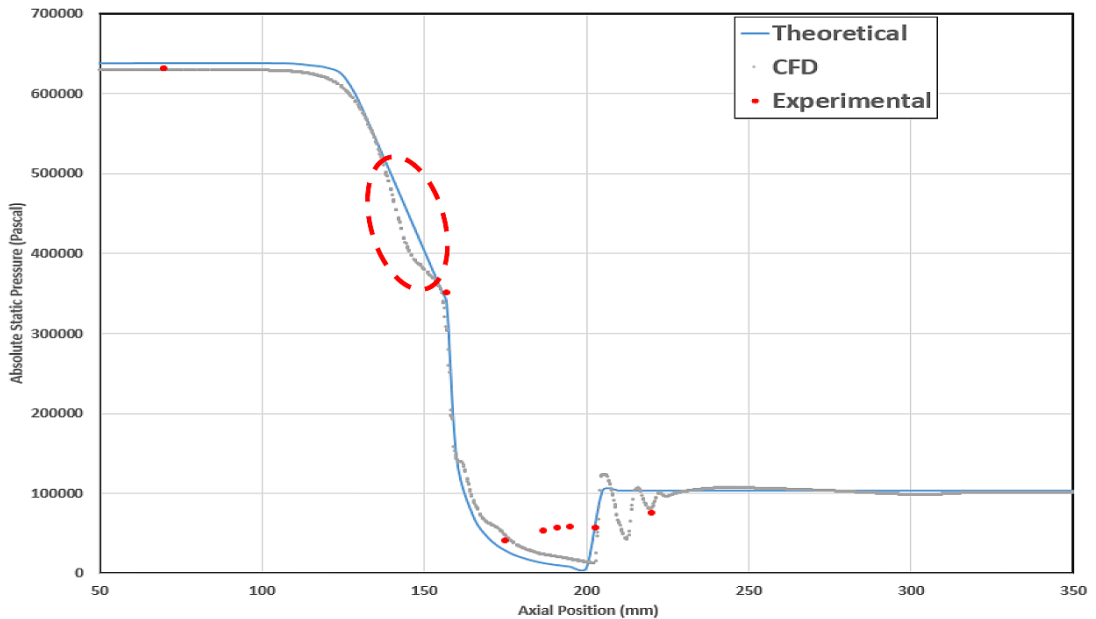
### 5.1 Pressure Results



Figure 4 - Axial Pressure distribution for Inlet Pressure of 5.3 Bar (Gauge)

Throughout the Subsonic region, there are two experimental data points which agree completely with the theoretical and CFD results. Similar to the Mach number data, there seems to be no effect from compressibility as this would tend to affect the experimental data point at ~155mm (throat). The theoretical and CFD results are extremely similar although there is a region of interest, encircled in red above. The region shows a slight drop of pressure compared to the theoretical results.

The supersonic flow region exists from around 155mm until the apparent shock formation around 200mm. As can be seen, the theoretical and CFD results appear to fit seamlessly with no real exceptions which presents a high level of confidence in both the theoretical and CFD data. However, the experimental have a similar trend but trend but there is some discrepancy in values compared to both CFD and theoretical methods.

The experimental data prior to the shock wave is in the correct region and appears to jump slightly to the correct post-shock value as proposed by the theoretical and CFD data. The results, although they are in the correct region do not provide full confidence as the pressure does not produce as much of a spike as originally proposed by the theoretical tool and CFD simulation

The data sets from the other tests, with different inlet pressures, also fit extremely well which increases the confidence between the methods of calculation.
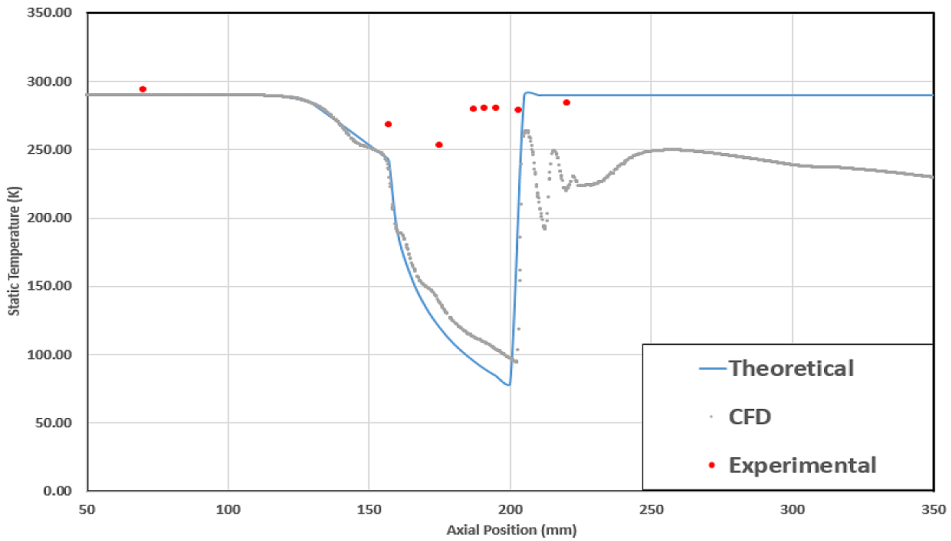
## 5.2 Temperature Results



Figure 5 - Axial Temperature distribution for Inlet Pressure of 5.3 Bar (Gauge)

It can be seen that the experimental temperature data in the graph is not conclusive. The theoretical and CFD data before the shock agree very well, providing an identical reading for shock location and as such, provide some confidence in both. The CFD, due to its higher accuracy and more realistic calculations produce a slight gradual reduction of temperature upon approach to the shock in which would be expected in reality.

It is clear however aft of the throat (where the airflow > Mach 1, around 155mm) that the experimental data does not fit the strong trend represented by the theoretical and simulation data, which reduces confidence in the measuring method/ equipment. It is extremely clear that the experimental measurement of temperature was extremely sensitive to placement of the thermocouple and therefore are not fully representative of realistic figures, leading to the values that were gathered in the Figure 5.
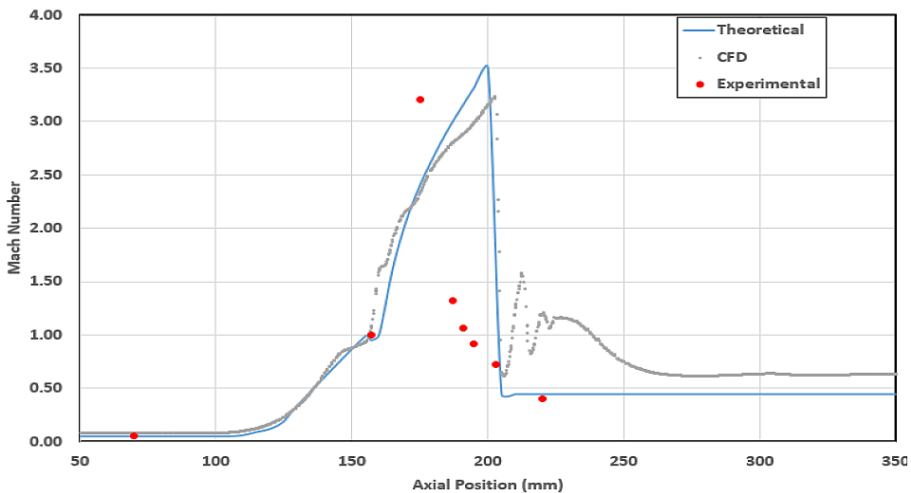
## 5.3 Mach Number Results



Figure 6 - Mach number distribution for Inlet Pressure of 4.5 Bar (Gauge)

As can be seen Figure 6 the subsonic flow values for each stream of data agree completely. This is primarily down to majority of the flow in the convergent portion being incompressible and which lends itself to 'ideal', isentropic calculations. The isentropic relationships appear to be extremely consistent (across the full range of pressures) in calculating the flow characteristics seen in this nozzle, even when approaching the hypersonic flow region (~Mach 4). As compressibility and other effects related to supersonic flows become a factor, the data is still in general agreement as the flow reaches around Mach 3. Towards the end of the region annotated 'Supersonic Region', at an axial position of around 175-200mm, the theoretical and CFD data sets begin to diverge slightly, which is primarily caused by the over simplicity of the theoretical model assuming that there is no gradual decrease of fluid velocity as the upstream shock is approached. In reality, there is a gradual decline of velocity and this is shown by the gradual deceleration of the Mach number in the CFD results. The results in this region do agree very well and produce very similar trends as well as the peak Mach number being within an acceptable tolerance.

The experimental values, however, do not appear to agree completely with the Mach numbers calculated via theoretical and CFD models and appears to be ~0.75 Ma higher than its theoretical/CFD counterpart. This leads to reduced confidence in the experimental rig as the theoretical and CFD values are so closely in agreement. It can be explained by the fact that the temperature measuring device (upon which the Mach number is heavily dependent) is not accurate enough. However, the experimental data does follow all major trends and does show a gradually declining Mach number that eventually rests at a similar value to the theoretical calculation. Another important aspect in the agreement of results is the shockwave region, which is represented almost identically by the theoretical and CFD results. Both share a clear, instantaneous drop in Mach number at an axial position of ~200mm. This drop is not so evident in the experimental data and appears more gradual, this is most likely due to the experimental values providing a heavily-averaged set of values compared to the theoretical/simulation data. The CFD results do not provide a clean drop, like the theoretical values, and some quite powerful oscillation is present aft of the shock.

### 5.4 Shockwave Boundary Layer Interaction (SBLI)

As can be seen throughout the results, and is especially clear in the Fluent results for TEST 1 at 5.3 Bar (Gauge), there is some high-level flow phenomena occurring in the divergent section of the nozzle. It can be seen that a region of normal and oblique shocks is produced where it is known, throughout the results, that the flow undergoes a severe spike in pressure & temperature, coupled with a severe reduction in Mach number (to subsonic).
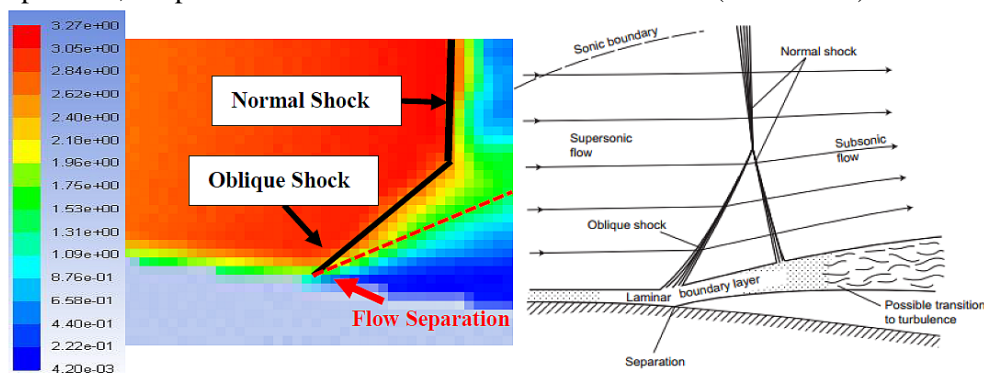


Figure 7 - Comparison of CFD Mach Contours (Test 1 @ 5.3 Bar) with Theoretical Diagram from [13]

A detailed view of separated flow's turbulent energy contours (shown in Figure 8)) confirms the theoretical hypothesis that the separate flow may transition to turbulence after the SBLI. It can be seen in the figure that the Turbulent Kinetic Energy spikes to ~18,700 $m^2/s^2$ after the point of flow separation. Denoting a definite turbulent transition.
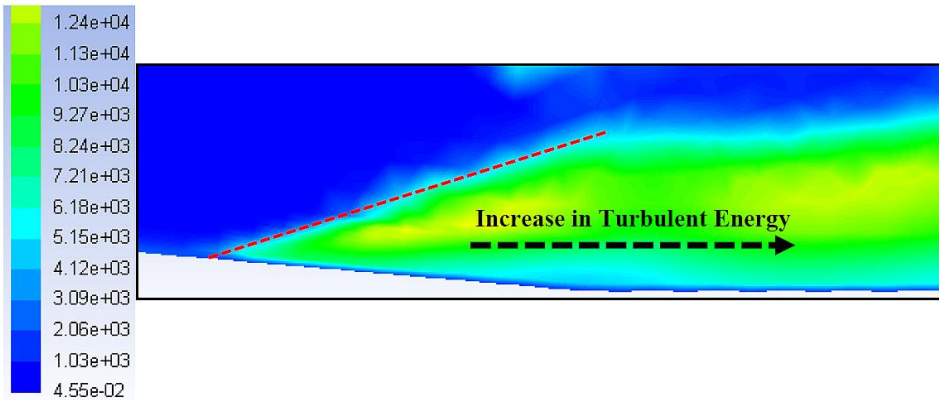


Figure 8 - Turbulent Kinetic Energy Contours of CFD Results showing a Definite Transition to Turbulence after SBLI

## 6. CONCLUSIONS

The results in Figs 4, 5 and 6 show that there are some discrepancies in the results from theoretical analysis and CFD predictions. This may be attributed to the detailed calculation of the CFD method compared to theoretical method which based on a single value at each cross-section. The convergence criteria used may another source of difference in results. Regarding the discrepancy between the experimental results and both CFD and theoretical methods, this may be refereed to accuracy of sensors and instrumentation used to collect the data, the testing procedure, compressibility effect and shock-boundary layer interaction. The response time for both pressure and temperature sensors is high due to the thermal and deflection working principle of the thermocouples and pressure diaphragm sensors. The sensors response time could the main source of error in temperature and pressure measurements.

The Excel-based 'Shockwave Location' Tool played its part in the research by initially providing the information needed for a successful modifying the experimental rig and then providing information upon which conclusions were able to be formed. The Excel tool appears to have a range of effectiveness which begins to diminish slightly at Inlet Pressures of below 3.5 Bar (Gauge) [4.5 Bar Absolute/ Pressure Ratio of 4.5] allowing for more work to be undertaken in order to increase its range of effectiveness by revisiting the original equations used and tailoring them to accommodate for the effects of lower pressure flows.

As the basis for the project, the nozzle rig provided this research with another stream of data to increase confidence in the CFD model. I believe that the nozzle rig has achieved its sole purpose and effectively enriches the project's conclusions. The nozzle rig however, can still be improved and in order to further increase confidence in the data it provides, more accuracy would need to be instilled through the base rig geometry and also the measuring equipment and processes. The main output of this research, the CFD Model of the Nozzle, is extremely robust and more-than-sufficient degree of accuracy for most applications. Full investigations into the optimum turbulent model and correct turbulent boundary conditions may results in a higher-accuracy model but was deemed outside of the scope of this research.

The research has established a robust CFD model which can be used to analyse other candidate nozzle designs with confidence. Other designs may have benefits over that which has been analysed throughout this research due to certain designs requiring less complex manufacture and also more versatility. It is necessary to point out that this research can still be infinitely expanded upon for further impact on the field of CFD.

# REFERENCES

[1] A. A. Khan, Shembhakar, Viscous Flow Analysis in a convergent-divergent nozzle, *International Conference on Aerospace Science and Technology*, Bangalore, 2008.

[2] S. C. Asbury, C. L. Gunther, C. A. Hunter, *A passive cavity concept for improving the off-design performance of fixed-geometry exhaust nozzles*, 32nd Joint Propulsion Conference and Exhibit, pp. 96-2541, 1996.

[3] Q. Xiao, H. M. Tsai, D. Papamoschou, Numerical investigation of supersonic flow separation, *AIAA Journal*, **45**, pp. 532-541, 2007.

[4] R. Boyanapalli et al, Analysis of Composite De-Laval Nozzle Suitable for rocket applications, *International Journal of Innovative Technology and Exploring Engineering*, **2**, pp. 336-344, 2013.

[5] S. E. Rafiee, M. M. Sadeghiazad, Experimental and 3D CFD analysis on optimization of geometrical parameters of parallel vortex tube cyclone separator, *Aerospace Science and Technology*, **63**, pp. 110-122, 2017.

[6] G. Cai, J. Fang, X. Xu, M. Liu, Performance Prediction and Optimisation for Liquid Rocket Engine Nozzle, *Aerospace Science and Technology*, **11**, pp. 155-162, 2007.

[7] V. Lijo, H. D. Kim, T. Setoguchi, S. Matsuo, Numerical simulation of transient flows in a rocket propulsion nozzle, *International Journal of Heat and Fluid Flow*, **31**, pp. 409-417, 2010.

[8] K. Pougatch, M. Salcudean, E. Chan, B. Knapper, Modelling of compressible gas–liquid flow in a convergent–divergent nozzle, *Chemical Engineering Science*, **63**, pp. 4176-4188, 2008.

[9] A. Balabel, A. M. Hegab, M. Nasr, S. M. El-Behery, Assessment of turbulence modeling for gas flow in two-dimensional convergent–divergent rocket nozzle, *Applied Mathematical Modelling*, **35**, pp. 3408-3422, 2011.

[10] M. Grujicic, et al., Analysis of the impact velocity of powder particles in the cold-gas dynamic-spray process, *Materials Science and Engineering*, **A368**, pp. 222-230, 2004.

[11] * * * NASA, *Normal Shock Wave Equations*, [Online] Available at: https://www.grc.nasa.gov/www/k-12/airplane/normal.html[Accessed April 2017], 2015.

[12] J. Green, Interactions between shockwaves and turbulent boundary layers, *Program of Aerospace Sciences*, **11**, pp. 235-240, 1970.

[13] P. Doerffer, O. Szulc, F. Magagnato, Unsteady Shock Wave-Turbulent Boundary Layer Interaction in the Laval Nozzle, *Task Quarterly (Scientific Bulletin of the Academic Computer Centre in Gdansk)*, **9**(1), pp. 115-132, 2004.

[14] E. L. Houghton, P. W. Carpenter, S. Collicott, D. Valentine, *Aerodynamics for Engineering Students*, 6. Edn., ed. Aerodynamics for Engineering Students. New York: Butterworth-Heinemann, pp. 588-591, 2013.

[15] J. D. Anderson, *Compressible Flow Through Nozzles*, in: Introduction to Aerodynamics, New York: McGraw-Hill, pp. 510-530, 1996.

[16] R. S. Vajjha, D. K. Das, P. K. Namburu, Numerical study of fluid dynamic and heat transfer performance of Al2O3 and CuO nanofluids in the flat tubes of a radiator, *International Journal of Heat and Fluid Flow*, **31**, pp. 316-321, 2010.

[17] A. Hadjadj, Y. Perrot, S. Verma, Numerical study of shock/boundary layer interaction in supersonic overexpanded nozzles, *Aerospace Science and Technology*, **42**, pp. 158-168, 2015.

[18] Y. Allamaprabhu, B. N. Raghunandan, J. A. Morinigo, Numerical prediction of nozzle flow separation: Issue of turbulence modeling, *Aerospace Science and Technology*, **50**, pp. 31-43, 2016.

[19] J. Wu, X. Liu, R. Radespiel, RANS simulations of a tandem nozzle supersonic wind tunnel, *Aerospace Science and Technology*, **49**, pp. 215-224, 2016.